



Research Article

A starch-assisted innovative synthesis of spinel-structured and ferromagnetic behaviour of Fe_3O_4 nanoparticles catalytic activity evaluated in the selective oxidation

V. T. Geetha^{1,2} · G. Puthilbai^{1,2} · S. Induja¹

© Springer Nature Switzerland AG 2019

Abstract

In this research work, for several temperature based on Fe_3O_4 nanoparticles had been prepared by the sol–gel approach. The physicochemical properties of these catalysts were characterized by the X-ray diffraction (XRD), scanning electron microscopy, transmission electron microscopy (TEM), diffused reflectance spectra, photoluminescence spectroscopy (PL) and vibrating sample magnetometer. Fe_3O_4 nanoparticles, TEM images and the XRD analysis designated that the chain-like Fe_3O_4 has a crystal phase of cubic lattice by way for a mean measurement of around 25 nm. The effect of catalyst and solvent on the catalytic oxidation of benzyl alcohol using the Fe_3O_4 catalyst prepared by sol–gel method was also investigated.

Keywords Nanoparticles · Magnetic materials · Starch · Sol–gel

1 Introduction

Fe_3O_4 was known as an important semiconductor which has been studied extensively in the past few years because of its fundamental and technological advantages. The fundamental residential properties among these nanostructured materials depend on their architectures geometry that is containing morphology and hierarchical structures. Therefore, the control of shapes and sizes with the semiconductors to get desired properties is one of the most inspiring topics presently challenged by the material science. Specially, over the past few years, much effort is made to develop novel methods to prepare nanostructured metal oxides chalcogenide semiconductors [1]. Magnetite (Fe_3O_4) through the inverse that is cubic spinel structure has displayed unique electric, optical, catalytic therefore the magnetic properties using the transfer of electrons between Fe^{2+} and Fe^{3+} in the octahedral sites. Furthermore, the iron oxides presented extraordinary multiplicity in terms of the oxidation state, Fe^{2+} could act as

bridging ions to Fe^{3+} has a larger charge valence than divalent cations, therefore Fe^{3+} could connect the activated sludge more strongly and endure greater shear forces, causing the particle dimensions to be larger compared with divalent ion [2, 3].

Fe_3O_4 nanopowder is made by the many techniques like hydrothermal method [4], sonochemical process [5], citrate–nitrate [6, 7] and sol–gel method [8], prepared form metal oxides. The present work, that the sol–gel method includes that the conversion for monomers interested in as a colloidal solution (sol) that the performances as the precursor for an integrated net-work (or gel) of whichever separate particles or network is attained metal oxides. The sol progressively changes towards the formation for gel-like diphasic organization for containing both liquid and the solid phases whose morphologies range from discrete particles near continuous networks for heated treatment on your way for synthesizes products n this chemical process.

✉ V. T. Geetha, geethavt@yahoo.com | ¹Hindustan Institute of Technology and Science, No: 1, Rajiv Gandhi Salai (OMR), Padur, Chennai 603103, India. ²Department of Chemistry, Sri Sairam Engineering College, Sai Leo Nagar, West Tambaram, Chennai 600044, India.

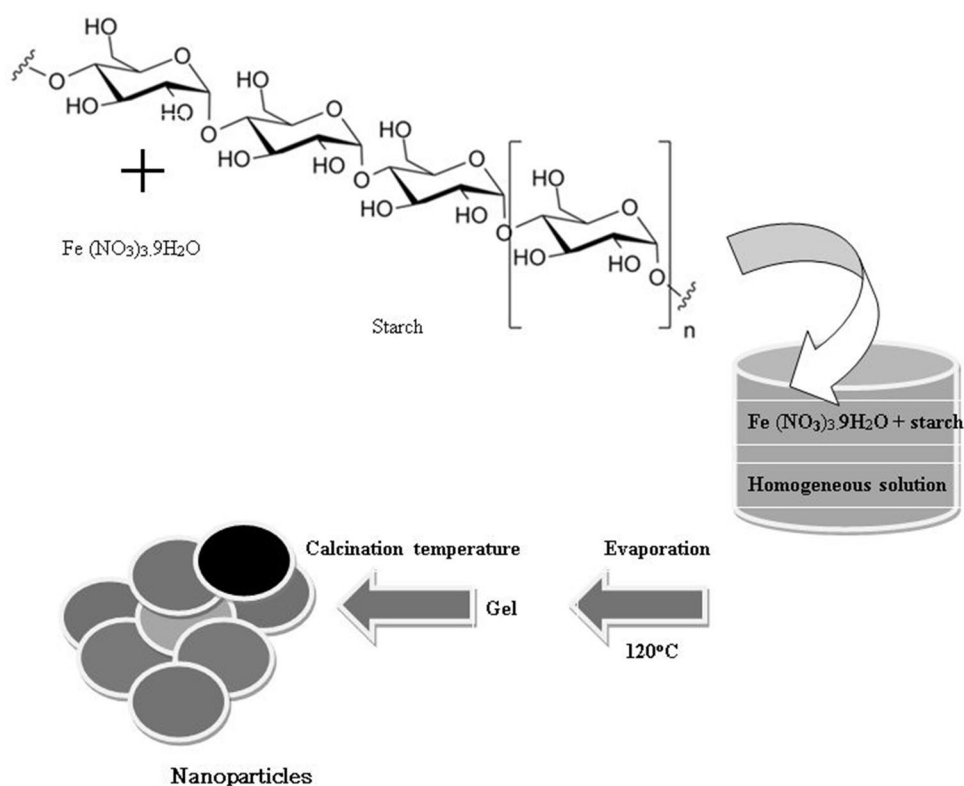


SN Applied Sciences (2019) 1:472 | <https://doi.org/10.1007/s42452-019-0450-3>

Received: 30 December 2018 / Accepted: 2 April 2019 / Published online: 19 April 2019

SN Applied Sciences
A SPRINGER NATURE journal

Scheme 1 Schematic diagram of the formation process of Fe_3O_4



The current work is a new effort. It is noteworthy that it is the first time that the effects of fuels or capping agents (including amounts of reductant, molar ratios calcination temperature within time) on crystal size, shape, phase and the structure, magnetic, catalytic oxidation toluene to benzaldehyde for Fe_3O_4 nanoparticles are investigated.

2 Experimental

2.1 Materials

All research work, reagent grade MDEA (> 99% pure) starch, $\text{Fe}(\text{NO}_3)_3 \cdot 9\text{H}_2\text{O}$, were used as received without further purification.

2.2 Synthesis

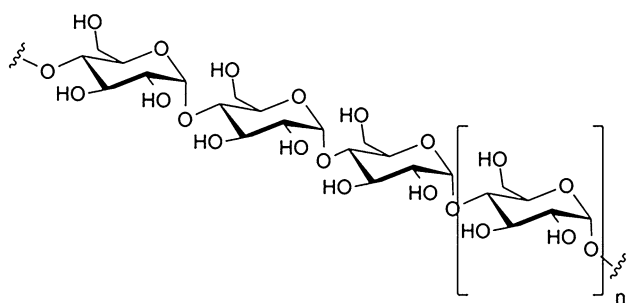
In an ordinary experiment, starch was dissolved in 20 ml hot distilled water and the $\text{Fe}(\text{NO}_3)_3 \cdot 9\text{H}_2\text{O}$ of 50 ml was dissolved in water were used for molar ratio (1:2). In the second stage, the two solutions were mixed, positioned in a 100 ml beaker and the homogeneous solution obtained was transparent and it turned into an exceedingly viscous transparent gel at 80 °C which was dried on hot plate at 120 °C for 6 h. In this stage, the thermal processing in air atmosphere (300,400 and 500 °C/3 h) in order to remove

the carbonaceous material and the spherical like nanoparticles formation of Fe_3O_4 (Scheme 1) is presented as samples, such as, A (300 °C), B (400 °C) and (500 °C) C. Nowadays, starch have been used as both reducing and gelling agent for the synthesis of nanomaterials, which could be advantageous over phytochemical reduction, heat evaporation, and other chemical reduction methods. The starch is then defatted before use. This is termed "native starch" and has no modification whatsoever. Therefore, (Scheme 2) sucrose can also act as an effective chelating agent like starch to produce fine particles. By the using starch [amylopectin (normally 70–80%)] as a fuel.

Metal oxides synthesis of nanostructures Fe_3O_4 using starch as a reducing agent. The slow reduction of the nanomaterials along with the shape directing effects of the constituents of the starch plays a key role in the formation of the metal-oxide. Due to the desire for eco-friendly processes, new green synthesis using starch has acquired greater importance.

2.3 Characterization

A diffract meter with X'Pert Pro mono chromatized Cu K α radiation ($k = 1.54 \text{ \AA}$) of Philips Company was used to collect XRD patterns. FE-SEM and TEM images were obtained on MIRA3 FEG-SEM and JEM-2100 with an accelerating voltage of 60–200 kV equipped with a high-resolution



Scheme 2 Structure of amylopectin

CCD camera, respectively. The absorption and the emission properties were recorded using Varian Cary Eclipse Fluorescence spectrophotometer. The magnetic behavior at room temperature was studied by the vibrating samples magnetometer (VSM 7403, Lakeshore, USA) in a field up to 710 kOe. The nitrogen adsorption–desorption isotherms of the samples were measured by using an automatic adsorption instrument (Quantachrome Quadrawin gas sorption analyzer) for the determination of the surface area and total pore volume.

2.4 Catalytic tests

In order to investigate the activity of Fe_3O_4 as a catalyst for the oxidations of toluene. Fixed batch reactor, which operated under atmospheric conditions of 5 ml of CH_3CN ; 5 mmol of oxidant (H_2O_2) was added along with 0.3 g of the Fe_3O_4 , and the contents were heated at 80°C in an acetonitrile medium for 8 h in a three-necked round bottom flask equipped with a reflux condenser and thermometer. The oxidized products after the catalytic reaction were collected and studied using an Agilent GC spectrometer. The column used for the study was DB wax column (capillary column) of length 30 mm, and helium was used as the carrier gas.

3 Results and discussion

3.1 XRD spectra

X-ray diffraction examination of the produced powder heated up in atmosphere at different temperatures, such as, 300°C , 400°C and 500°C included revealed in Fig. 1a. Most of the detectable peaks to be perfectly indexed to cubic Fe_3O_4 to spinel-structured with cell constants $a = 8.393 \text{ \AA}$ (JCPDS 85-1436). It is noticed that the strong and sharp reflection peaks became sharper with increasing calcination temperature, indicating the enhancement of crystallinity. Fe_3O_4 is observed through the gradual

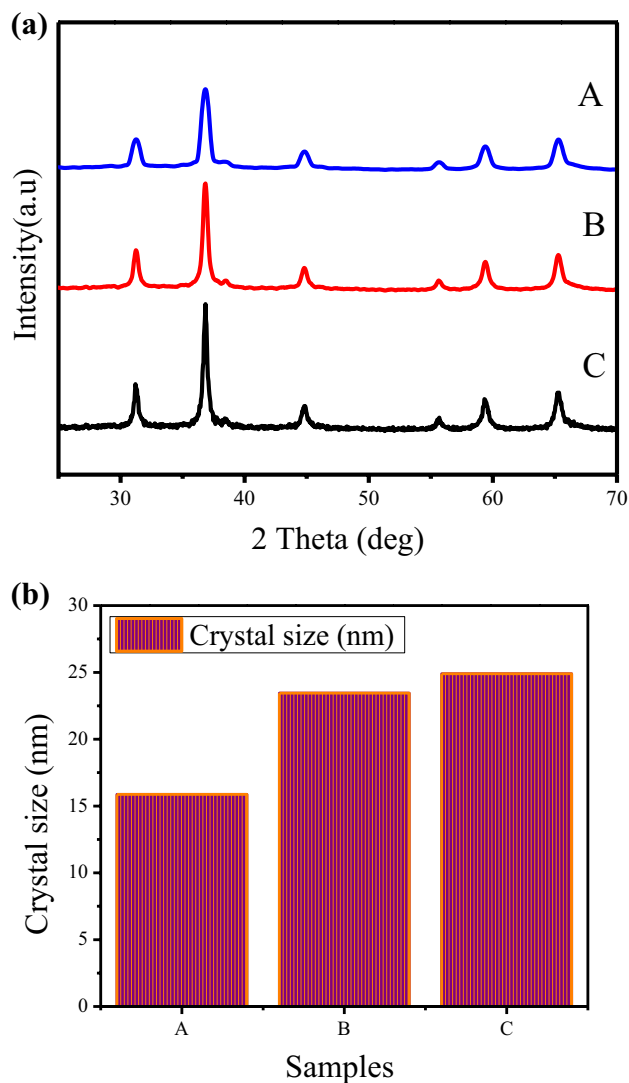


Fig. 1 **a** XRD pattern of Fe_3O_4 nanoparticles prepared by sol–gel method. **b** Average crystal size shows Fe_3O_4 nanoparticles samples A, B and C

increase temperatures in the peak intensities accompanied by sharpening of the peaks. The average crystallite size (around 30 nm) in the powders was calculated by using Debye–Scherrer’s equation. The average crystal size of Fe_3O_4 as shown in Fig. 1b in the nanoparticles made, are seen to be, slighter compared to diameters associated with the spherical-like particles for temperature influences.

The average crystallite size was estimated by the applying the Scherrer formula [12] on the highest intensity peak for each sample.

$$L = \frac{0.89\lambda}{\beta \cos \theta}$$

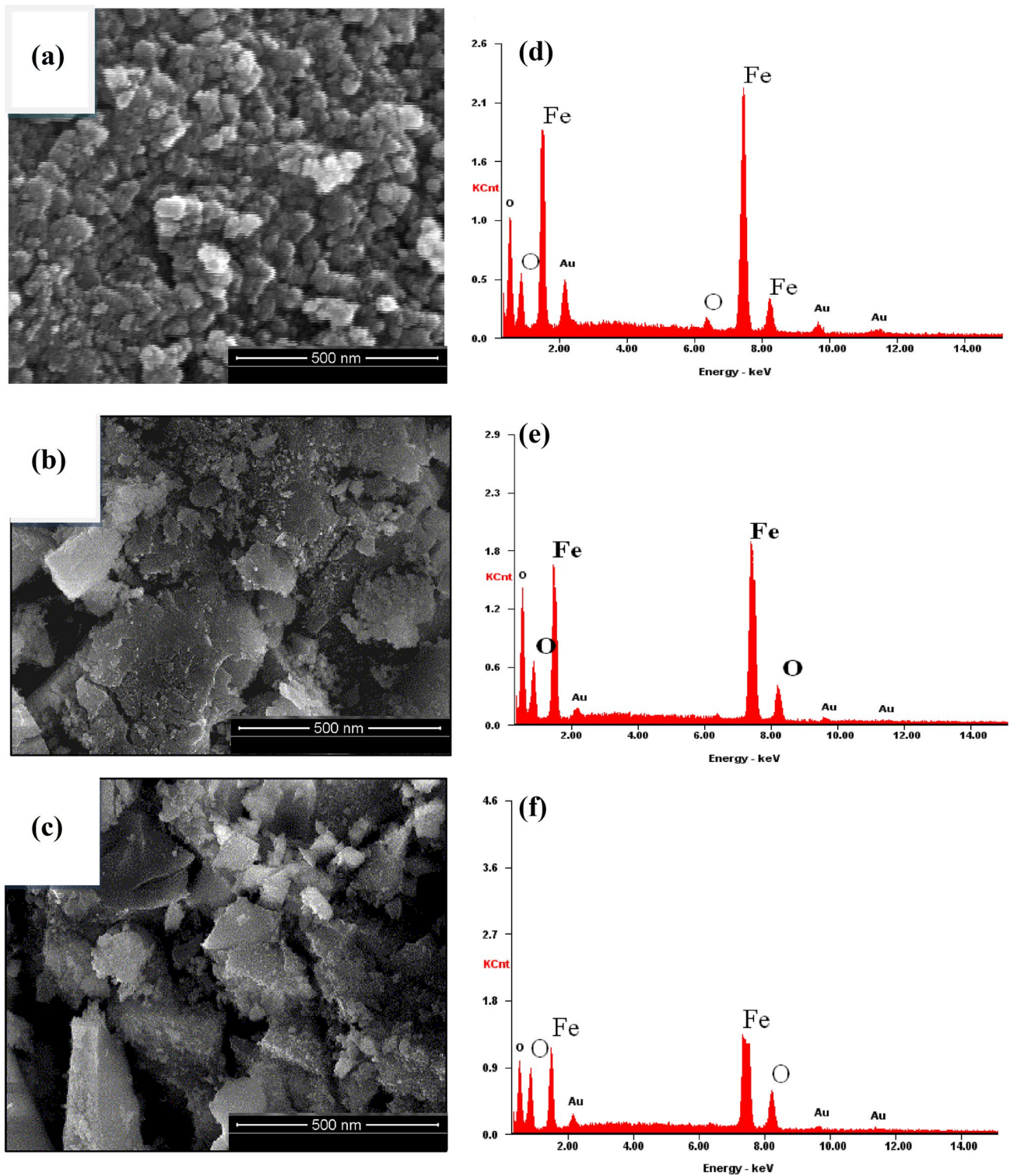


Fig. 2 a–c HR-SEM images of Fe₃O₄ nanoparticles. d–f EDX spectra shows Fe₃O₄ nanoparticles

where L is the average particle size, β , the full width at half maxima (FWHM), θ , the Bragg angle and λ , the wavelength of (0.154 nm) Cu-K α in radians.

3.2 Morphological analysis

Surface morphological associated with the Fig. 2 Fe₃O₄ nanoparticles was performed by using SEM images.

Through the SEM image was actually seen that the nanoparticles had been agglomerated, particles of grain dimensions by having with a range of 15–30 nm. Meanwhile, with growing temperatures regarding the particle's proportions showed thick agglomerate it is resonances. Figure 2 presentations for EDX spectra on Fe_3O_4 nanoparticles attained from the samples as well peaks for Fe and O elements and there were no peaks for other impurities. The transmission electron microscopic (TEM) photographs with the product has been considering in Fig. 3. The particle size nanoparticles obtained from the XRD diffraction designs are in nearby agreement with the TEM analysis which showcase dimensions of 20–30 nm. The crystallite size is in arrangement with that obtained from XRD research analysis (30 nm). The temperature got discovered to play a role that is key the synthesis of nanocrystalline Fe_3O_4 . TEM images indicate that Fe_3O_4 powders consists of nanometric particles, nanoparticles obtained from samples with starch (fuel) were found to have slightly smaller particles with respect to the sample, which is in good agreement with XRD. To investigate the size distribution of the nanoparticles particle size histograms were prepared for the Fe_3O_4 nanocrystals annealed at 300–500 °C. The information was obtained by measuring every nanoparticle on the TEM images of the same sample (80 nanoparticles). Most of the particles have 16–19 nm sizes for Fe_3O_4 samples (300–500 °C) with 17–30 nm for the obtained products. Further observation at higher magnification reveals that each nanobundles actually consists of nanoparticles that are individually ca. 20 nm in diameter.

3.3 Vibrating sample measurements (VSM)

The magnetic belongings from the Fe_3O_4 samples at (A) 300 °C, (B) 400 °C and (C) 500 °C stayed reported by the using of vibrating sample magnetometer (VSM). The room temperature with the applied field ranging up to ± 10 kOe is shown in Fig. 4a, in which noticeably designated that the prepared samples (A, B and C) can be detached from liquid by the applying of external field that is magnetic nature. Whenever the sample is actually cooled off in zero magnetic fields the magnetization that is total zero since the magnetic dipoles of the associated with particles become randomly driven. VSM results of saturation magnetization (Ms), remanent magnetization (Mr) and coercivity (Hc) values are reported in Table 1. Magnetic hysteresis (M-H) loop demonstrations both the samples possess ferromagnetic conduct with gentle that is magnetic. Magnetic anisotropy may be the significant influence to recognize the ferromagnetic properties. We found that the Fig. 4b shows the magnetic properties are construction and therefore dimensions in dependent on method. Supplementary

more important, standards of Ms, Mr, Hc therefore the morphology of products obviously depend on the precursor that is utilized that are the fundamental points for functional solutions [9, 10]. No structural or magnetic phase transition consumes continued below Fe_3O_4 samples A, B and C. Consequently, the experiential unequal variation that the H_c through the temperature extreme probable remains owing to anomalous difference between for magneto crystalline anisotropy with (the anomalous temperature variation of coercivity (i.e., decrease in Hc with decreasing temperature)) temperature factor in the present scenario.

3.4 DRS properties

In order to control of optical characteristic of the fashioned Fe_3O_4 nanoparticles, the UV–Vis Spectra (with DRS) was obtainable in Fig. 5. In the current learn, the solitary absorption was observed in three products, which designates the growth on a single-phase ingredient. The absorption peak (λ_{max}) that the originate of shifted nearby the reduced wavelength lateral in case for any nanoparticles created through the method that is sol–gel designates that the absorbance (nm) is dependent on crystal/particle dimensions. The direct exceptional to the scenario that with decline in particle proportions the band gap increases [11].

3.5 PL spectra

For the research that is current, Fe_3O_4 nanoparticles PL spectra excited at wavelength of 390 nm substantial a strong peak at 528–536 nm (Fig. 6), in which the container continues to be accredited toward a high-level (energy) transition of Fe_3O_4 nanoparticles semiconductor materials. A diverse blue-green emission peaks at 530 nm and 545 nm remain connected toward an individually demonstrative oxygen vacancy, in which effects after the recombination for image produced hole through the duty condition of this particular area, such as for instance, oxygen positions, or resulted from the surface deep-level [12, 13]. Through the entire diffusion exciton then self-trapped, they are continuing to be an irradiative recombination, Fe and O ultimately causing luminescence, then you possible beginning on visible PL spectra.

3.6 Effect of functional groups

Figure 7 determines adsorption desorption isotherms on produced Fe_3O_4 at numerous calcined temperatures at 300 °C, 400 °C and 500 °C. Table 2 presentations the

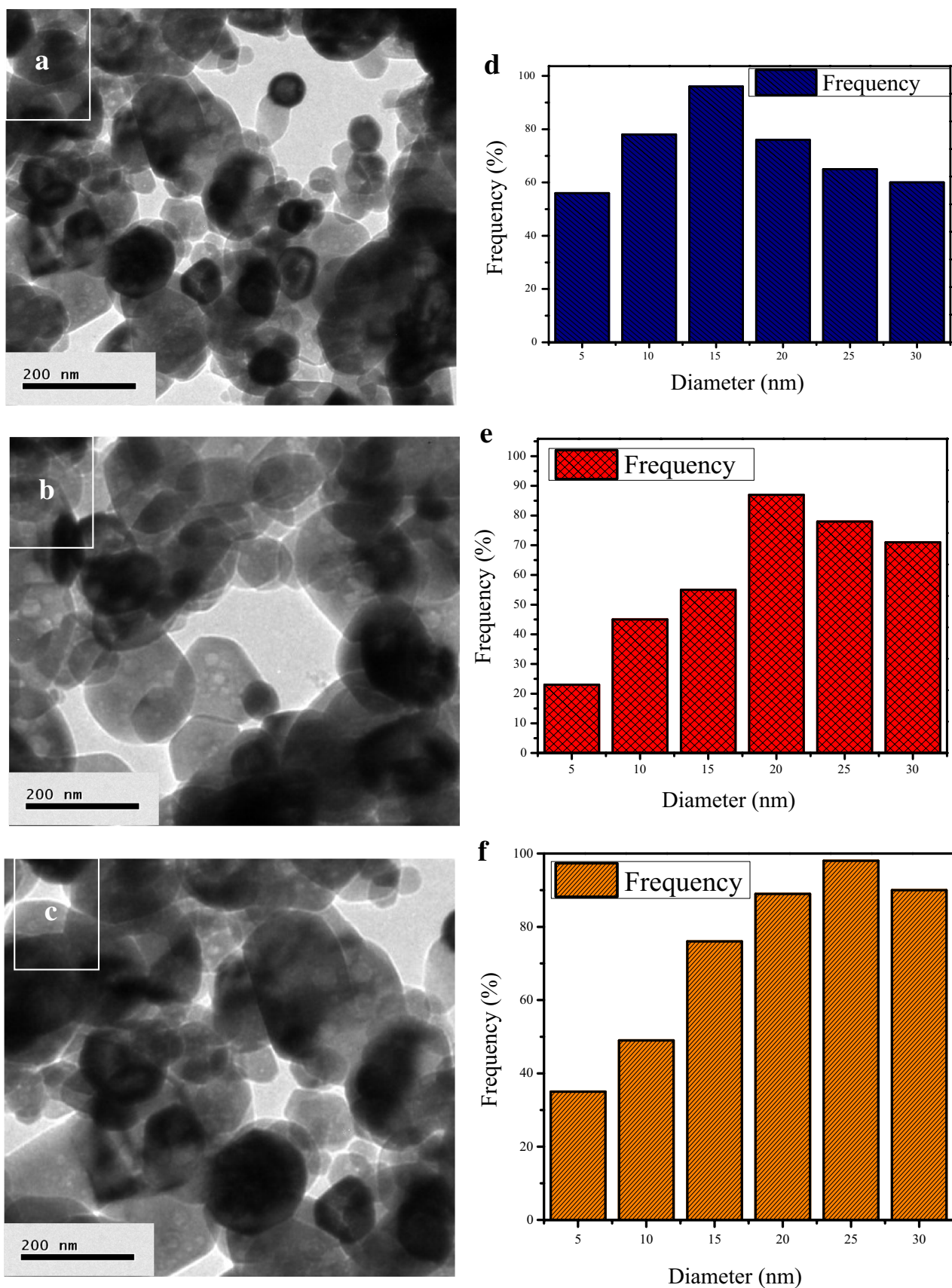


Fig. 3 a–c HR-TEM images of Fe₃O₄ nanoparticles. d–f Average particle size histogram of Fe₃O₄ nanoparticles

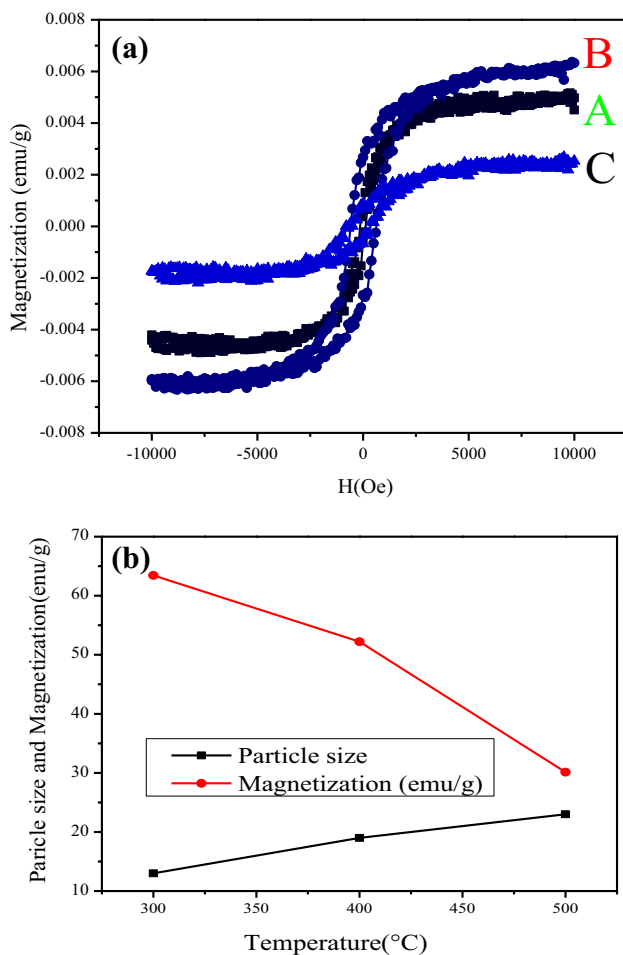


Fig. 4 **a** Room-temperature magnetic hysteresis loops of Fe₃O₄ nanoparticles. **b** Samples for temperatures VS particle size and magnetization

Table 1 Observed XRD and VSM data of the Fe₃O₄ samples (300, 400 and 500 °C) prepared by sol-gel method

Samples (°C)	Crystallite size (nm)	Coercivity (G)	Retentivity (emu/g)	Magnetization (emu/g)
300	13.68	18.73	6.467	73.45
400	17.34	16.10	2.732	69.21
500	23.45	15.76	2.231	60.12

surface area, particle size, pore volume and pore diameters for Fe₃O₄ acquired making use of stoichiometric amount of the starch. In current research work, the synthetic route employed in these research referrals excellent characteristics for the obtainment of powders with large surface area as well as an extremely porous structure at relatively reasonable preparation conditions. The high surface area in the highly porous structure of the created Fe₃O₄ finds possible submission as

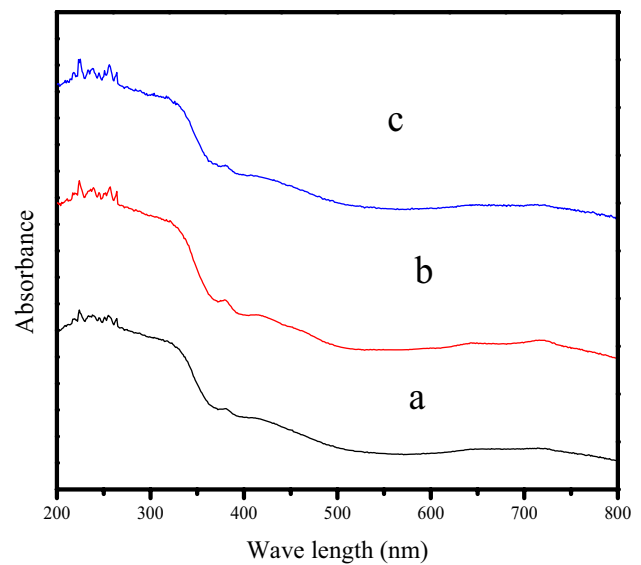


Fig. 5 Room temperature DRS spectra of Fe₃O₄ nanoparticles

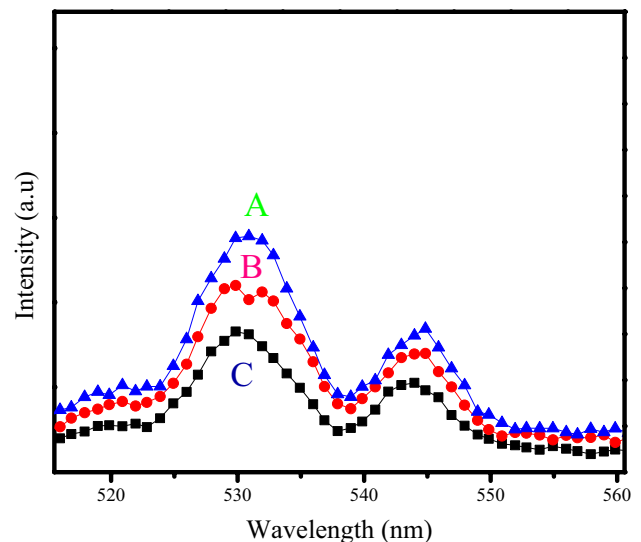


Fig. 6 Room temperature PL spectra of Fe₃O₄ nanoparticles

catalyst reaction or catalytic support. Generally speaking, researching these values aided by the agglomerate dispersal values, we located most fine particles that have a tendency to react with each other, reducing the high surface area therefore creating agglomerates of particles with comparable attributes (effortless agglomeration). From inside the present instance, high surface area and highly porous particles for Fe₃O₄ are of excessive significance for catalytic reasons given that it agrees with higher accessibility of reactant particles towards the catalyst and catalyst support reactions [14]. The data concerning pore size indicate that the pore size increases

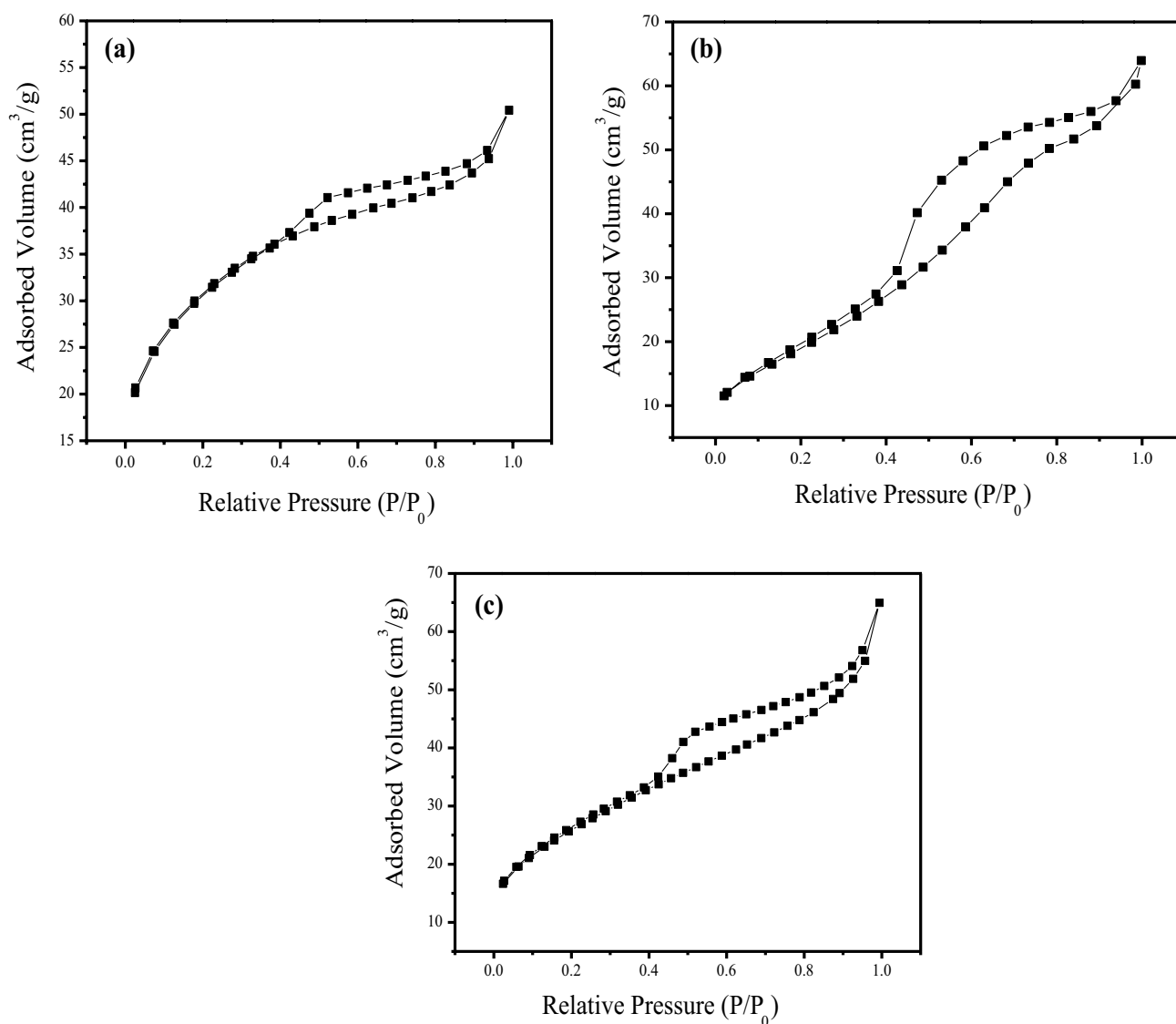


Fig. 7 N₂ adsorption/desorption isotherms of Fe₃O₄

Table 2 Surface area, pore volume and pore diameter of Fe₃O₄ catalysts

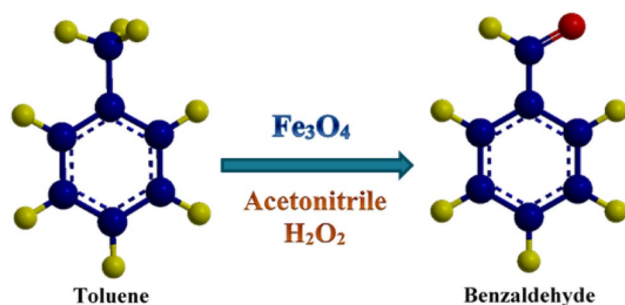
Properties	A	B	C
MultiPoint BET (surface area) (m ² /g)	107.3	83.73	62.84
Total pore volume for pores with radius (cc/g)	0.07799	0.09892	0.1005
Average pore radius (Å)	14.54	27.97	21.64

significantly with the reaction time, although the total pore volume was not practically altered. High surface areas were obtained for the samples calcined at 500 °C and also for the both samples calcined at 400 °C and 600 °C.

It was also observed that the surface area significantly decreases at higher calcination temperatures. In the SEM figures pores could be identified between the nanoparticles. These types of catalysts with high surface areas having narrow distributions of particles can be prepared by this soft chemical method. The compound prepared with such an excellent surface area may be promising for application as a catalyst.

3.7 Catalytic performances

We have examined the catalytic activity of Fe₃O₄ particles to be catalyst, for your oxidation of toluene using acetonitrile as a solvent therefore H₂O₂ as being an oxidant at the impulse heat of 80 °C, and effect times 8 h. Form inside



Scheme 3 Schematic representation for the oxidation of toluene

Table 3 Comparison of the catalytic performance in the oxidation of toluene

Samples	Conversion (%)	Selectivity (%)	Surface area analysis (m ² /g)
A	90	99	107.3
B	78	97	83.73
C	62	97	62.84

the catalytic reaction mixture, this product benzaldehyde ended up being receive to be oxidation product item as presented in Scheme 3. Generally, toluene oxidizes into benzyl alcohol, accompanied by benzaldehyde into benzoic acid. The selective oxidation will be the goal of the current research; benzaldehyde is targeted because the oxidation product is major. In current operate, catalytic presentation of as-prepared catalysts are evaluated from inside the discerning oxidation of benzyl alcohol using H₂O₂ as being an oxidant exhibitions the conversion process of toluene via benzyl alcohol and the selectivity of benzaldehyde as presented in Table 3. The above results showed that the as-prepared Fe₃O₄ nanoparticle catalysts tends to be promising catalytic materials when you look at discerning oxidation of toluene together with the better catalytic high recycling presentation and amazingly steady. The Fe₃O₄ catalyst found to have superior catalytic presentation in the selective oxidation of toluene among the catalysts. Highest yield had been gotten at room temperature while no other products (benzoic acid, benzyl alcohol) are developed as detected in majority of the stated processes.

Catalytic reaction time 8 h, solvent CH₃CN, oxidant H₂O₂ and necessary to achieve to the equilibrium. Figure 8 show that the carbonyl compounds was improved from 65 to 90% while amount catalyst was actually improved from 0.1 to 0.5 g but increase that is further perhaps not showcase any obvious effect for decrease in yields. Catalyst of amount 0.6 to 0.7 g increase in the therefore it also remained about unchanged when using high amounts

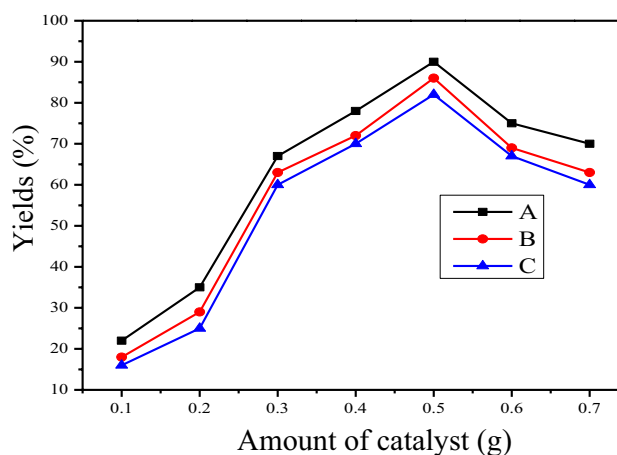


Fig. 8 Amount of catalyst of Fe₃O₄

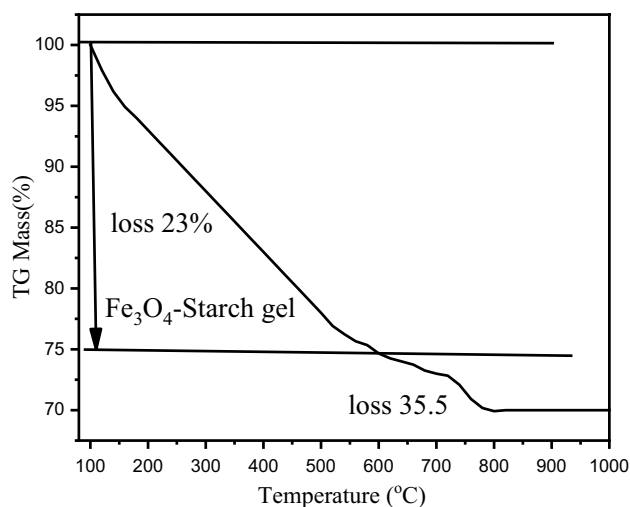


Fig. 9 TGA curves of Fe₃O₄

of the catalyst. The end results in the catalyst amount was actually examined to optimize the large yields with minimum level catalyst also to make the procedure that is whole reasonable. The counteraction of the catalyst plays a key role in the reaction-controlled phase-transfer catalytic system. This large increase indicates that the increase in catalytically active sites dramatically accelerated the conversion of the substrates. In our case, some catalytically active Fe₃O₄ species might not play a catalytic role at a high catalyst ratio because of the limited O₂ supply at atmospheric pressure. Lower conversion of benzyl alcohol with lower mass of catalyst was due to the fewer catalytic sites. Whereas, increasing catalyst mass beyond 80 mg, decreased the selectivity of benzaldehyde [15, 16].

3.8 TGA analysis

In order to evaluate the content of Fe_3O_4 in the Fe_3O_4 -starch-gel composite, thermogravimetric analysis (TGA) was conducted, and the result was shown in Fig. 9. synthesized by heat treatment from Fe_3O_4 -starch-gel composite. The mass loss ratio of pure Fe_3O_4 sample is 35.5%, and the mass loss ratio of Fe_3O_4 composite is 23%, results indicated that the composite contains approximately 70 wt% of Fe_3O_4 and 30 wt% of starch.

All the above results indicate that the preparation temperature has significant influence on the morphology and average size of Fe_3O_4 nanoparticles produced. 300 °C, it was found that the best results of the Fe_3O_4 nanoparticles synthesis, have been obtained when the reaction temperature is within this range. In other words, it was found that the best results of the Fe_3O_4 nanoparticles synthesis, have been obtained when the reaction temperature is within this range. Further temperature role, Fe_3O_4 grain size increases linearly with increase in the annealing temperature. This is due to an increase of atoms mobility and crystallite cross linking to form larger grains. The agglomerations of fine particles 19 nm are observed in the sample calcined below 300 °C. The small grains with approximately 22 nm in diameter are obtained by calcination at 400 °C, while the bigger grain size of about 30 nm is detected in the sample calcined at 500 °C. It is seen that the size of clusters in the samples slightly increases with increasing calcination temperature.

4 Conclusion

Present work perseverance creates a submission that is promising for eco-friendly synthesis on the carbonyl compounds. The forming of spherical shaped nanoparticles that are hexagonal-like around them is shown by SEM and TEM. The synthesis of Fe_3O_4 normally verified by EDX comparison. Fe_3O_4 nanoparticles confirmed great optoelectronic properties. Therefore, improvement effective catalyst providing high yield and selectivity under optimal conditions and without causing environmental and ecological pollutions is of great advantages for any modern chemical industry.

Acknowledgements We acknowledge the support extended by Sri Sairam Engineering College, Hindustan Institute of Technology and Science, India for providing research facilities.

Compliance with ethical standards

Conflict of interest The authors declare that they have no competing interests.

References

- Xiao ZL, Han CY, Kwok WK, Wang HH, Welp U, Wang J, Crabtree GW (2004) Tuning the architecture of mesostructures by electrodeposition. *J Am Chem Soc* 126:2316–2317
- Park J, Lee E, Hwang NM (2005) One-nanometer-scale size-controlled synthesis of monodisperse magnetic iron oxide nanoparticles. *Angew Chem Int Ed* 44:2872
- Ren X, Chen Y, Guo L, She Z, Gao M, Zhao Y, Shao M (2018) The influence of Fe^{2+} , Fe^{3+} and magnet powder (Fe_3O_4) on aerobic granulation and their mechanisms. *Ecotoxicol Environ Saf* 164:1–11
- Fu YS, Chen Q, He MY, Wan YH, Sun XQ, Xia H, Wang X (2012) Copper ferrite-graphene hybrid: a multifunctional heteroarchitecture for photocatalysis and energy storage. *Ind Eng Chem Res* 51:11700–11709
- Karunakaran C, SakthiRaadha S, Gomathisankar P, Vinayagamoorthy P (2013) Nanostructures and optical, electrical, magnetic, and photocatalytic properties of hydrothermally and sonochemically prepared $\text{CuFe}_2\text{O}_4/\text{SnO}_2$. *RSC Adv* 3:16728–16738
- Li W, Li J, Guo J (2003) Synthesis and characterization of nanocrystalline CoAl_2O_4 spinel powder by low temperature combustion. *J Eur Ceram Soc* 23:2289–2295
- Zhang T, Zhu H, Croue JP (2013) Production of sulfate radical from peroxymonosulfate induced by a magnetically separable CuFe_2O_4 spinel in water: efficiency, stability, and mechanism. *Environ Sci Technol* 47:2784–2791
- Jin L, Qiu Y, Deng H, Li W, Li H, Yang SH (2011) Hollow CuFe_2O_4 spheres encapsulated in carbon shells as an anode material for rechargeable lithium-ion batteries. *Electrochim Acta* 56:9127–9132
- Ichiyanagi Y, Kimishima Y, Yamada S (2004) Magnetic study on Co_3O_4 nanoparticles. *J Magn Magn Mater* 1245:272–276
- Perdew JP, Wang Y (1992) Accurate and simple analytic representation of the electron-gas correlation energy. *Phys Rev B Condens Matter* 45:13244–13249
- Bhatt AS, Bhat DK, Tai C, Santosh MS (2011) Microwave-assisted synthesis and magnetic studies of cobalt oxide nanoparticles. *Mater Chem Phys* 125:347–351
- Vanheusden K, Warren WL, Seager CH, Tallant DR, Voigt JA, Gande BE (1996) Mechanisms behind green photoluminescence in ZnO phosphor powders. *J Appl Phys* 79:7983–7987
- Li Y, Cheng GS, Zhang LD (2000) Fabrication of highly ordered ZnO nanowire arrays in anodic alumina membranes. *J Mater Res* 15:2305–2309
- Santos PTA, Neiva LS, Leal E, Costa ACFM, Jesus AA, Andrade HMC, Gama L (2008). In: Proceedings of the 2nd international conference on ceramics, Verona, Italy (CDROM), vol 1, pp 1–6
- Han M, Yin X, Wu H, Hou Z, Song C, Li X, Zhang L, Cheng L (2016) Ti_3C_2 MXenes with modified surface for high-performance electromagnetic absorption and shielding in the X-band. *ACS Appl Mater Interfaces* 8(32):21011–21019
- Gong S, Jiang JZ, Shi P, Fan J, Xu Q, Min Y (2018) Noble-metal-free heterostructure for efficient hydrogen evolution in visible region: molybdenum nitride/ultrathin graphitic carbon nitride. *Appl Catal B Environ* 238:318–327

Publisher's Note Springer Nature remains neutral with regard to jurisdictional claims in published maps and institutional affiliations.